

## Emulsion glasses: A dynamic light-scattering study

Hu Gang,<sup>1</sup> A. H. Krall,<sup>2</sup> H. Z. Cummins,<sup>3</sup> and D. A. Weitz<sup>2</sup>

<sup>1</sup>*Exxon Research and Engineering Corporation, Route 22E, Amundale, New Jersey 08801*

<sup>2</sup>*Department of Physics and Astronomy, University of Pennsylvania, 209 S 33rd Street, Philadelphia, Pennsylvania 19104*

<sup>3</sup>*Department of Physics, City College of CUNY, New York, New York 10031*

(Received 11 June 1998)

A liquid-glass transition was observed experimentally in a new system, an oil-in-water emulsion. Dynamic light scattering was employed to obtain the intermediate scattering function  $f(q,t)$  for a range of volume fractions  $\phi$  and scattering vectors  $q$ . The results are compared with predictions of the mode coupling theory. While the usual idealized version of the theory provides accurate fits to the data on the liquid side of the transition, fits for volume fractions near the transition and in the glass phase were found to require the extended version, presumably due to an additional decay mechanism related to the deformability of the oil droplets. [S1063-651X(99)04901-6]

PACS number(s): 64.70.Pf, 82.70.Kj, 83.10.Pp

### INTRODUCTION

The liquid-glass transition occurs in a wide range of materials including the silicates, molecular liquids, molten salts, and polymers. At temperatures well below the glass transition temperature  $T_g$ , glasses are amorphous solids with non-zero shear modulus on any measurable time scale, while their structures exhibit no evidence of long-range order. It is generally (though not universally) believed that the glass transition is a purely kinetic transition, and that no thermodynamic phase transition is involved.

The hallmarks of the glass transition include extremely rapid increases in the shear viscosity and structural relaxation time with decreasing temperature, and the quenching in of disorder as the material undergoes an ergodic to nonergodic transition. While many experimental studies of these properties with a variety of experimental techniques have been reported, there is still no universally accepted theoretical explanation for the glass transition; experimental data continue to be analyzed with a variety of different theoretical models [1,2]. Thus further model systems that undergo a glass transition, and whose properties can be probed in detail, would be of great value to further elucidate this important transition.

Mode coupling theory (MCT) [3,4] has been very successful in explaining the evolving dynamics of the relaxation process in liquids approaching  $T_g$ , but comparisons of experiment and theory have generally been hampered by the complex structure of most real glass-forming materials. An important exception is provided by colloidal glasses for which the solid colloidal particles interact primarily via simple hard-sphere interaction potentials. In this case, particle volume fraction,  $\phi$ , plays the role of temperature as the thermodynamic variable which controls the onset of the glass transition. As  $\phi$  increases toward the glass transition, the viscosity of a suspension of colloidal particles diverges, and the frequency-dependent viscoelastic moduli can be well described within the framework of MCT [5]. Moreover, because colloidal particles typically have sizes of several thousand angstroms, light-scattering spectroscopy can directly probe the dynamics of these systems on the length scale

$qa \sim 1$ , where  $q$  is the scattering vector and  $a$  is the particle radius. Detailed dynamic light-scattering studies of colloidal glass formers have been reported and compared with the predictions of MCT, particularly by van Meegen and his co-workers [6–8] and by Bartsch and co-workers [9,10]. Since MCT calculations can be carried out with the important coupling constants evaluated explicitly for the hard-sphere system, the dynamics of colloidal glasses as probed by dynamic light scattering provide a possibility for direct comparison of experiment and theory with no adjustable parameters. There are, however, hydrodynamic interactions present in colloidal dispersions that are not included in MCT. To further explore the relevance of MCT to the liquid-glass transition, it is clearly desirable to investigate other systems for which the interaction potentials can be treated explicitly.

In this paper we describe a new system that, somewhat unexpectedly, exhibits the hallmarks of the glass transition. It is an emulsion consisting of two liquids—oil and water—with a small concentration of stabilizing surfactant. The oil is dispersed as surfactant-covered droplets in the continuous (water) phase, forming an emulsion. The emulsion droplets are further purified to make them monodisperse in size [11,12], making possible more detailed study of their behavior and more exact comparison to theoretical predictions of packing and dynamics. We show that this emulsion clearly undergoes a glass transition as the volume fraction of droplets,  $\phi$ , is increased. We study the glass transition with dynamic light scattering, and show that its behavior is well described within the formalism of mode coupling theory [3]. However, in marked contrast to the behavior of hard-sphere colloids, the extended version of MCT must be used for the emulsion, presumably reflecting the consequences of the deformability of the liquid droplets.

Besides providing a new system that can be used to test the validity of MCT, these data also provide important insight into the elastic properties of emulsions. As the droplet volume fraction increases, these emulsions undergo a pronounced transition from viscous fluids to highly elastic solids [12]. At the highest volume fractions, the shear modulus of the emulsions is controlled by the energy of deformation of the droplet shapes, or the surface tension [12]. The transition

to this behavior is governed by the deformation of the droplets, which first occurs at  $\phi_c \approx 0.64$ , or random close packing, the highest volume fraction at which undeformed spheres can be randomly packed. By contrast, the results presented here show that, in fact, these emulsions first become a solid at a significantly lower volume fraction,  $\phi_g \sim 0.58$ , determined by the colloidal glass transition, where the spatial packing of the droplets becomes so large that they are no longer able to freely move over all the space.

### EXPERIMENT

Our emulsions were comprised of silicone oil droplets in water, stabilized by sodium dodecylsulfate. The method of crystallization fractionation [11] was used to obtain monodisperse droplets with a radius of  $a \approx 0.25 \mu\text{m}$ . By replacing about half the continuous phase water with glycerol, we matched the indices of refraction of the droplets and continuous phase, thereby eliminating multiple scattering. The structure and dynamics of the emulsions could then be probed with light scattering, using the 514.5 nm line of an  $\text{Ar}^+$  laser. A desktop centrifuge was used to concentrate the emulsion to  $\phi \approx 0.7$ ; the excess solvent was removed, and then used to dilute the sample to the desired volume fraction which was set by careful control of the mass of the sample components, and was determined by drying and weighing the constituents of a portion of the concentrated sample. The emulsion clearly exhibited a sharp transition in its behavior with increasing  $\phi$ , going from a freely flowing fluid, to a very viscous fluid to a solid as  $\phi$  varied from about 0.5 to 0.7. Although the surface of the droplets is charged by the surfactant, the concentration of surfactant in the continuous phase is sufficient to reduce the screening length to a sufficiently small value that the droplet packing behaves very nearly as hard spheres. Nevertheless there is a very small difference between the phase volume fraction, which determines the phase behavior of the droplet packing, and the absolute volume fraction, determined by the weight of the constituents. For the droplets used in these experiments, this difference was less than 1% [12]; here, we quote the phase volume fraction.

The structure of the emulsions can be characterized by means of their structure factor  $S(q)$ , which can be measured quantitatively with static light scattering, because the droplets are monodisperse, and because they can be index matched to the solvent. The form factor of the individual droplets is first determined from the scattering intensity of a low volume fraction; this is used to normalize the measured scattering intensity from higher volume fractions, allowing  $S(q)$  to be determined. A typical example of  $S(q)$  for the samples used in these studies is shown in Fig. 1. It is obtained from a sample with  $a \approx 0.25 \mu\text{m}$  and  $\phi \approx 0.54$ , a volume fraction that is near the colloidal glass transition. The structure factor exhibits the typical behavior of a concentrated hard-sphere system. There is a pronounced peak at  $q_0 \sim 13 \mu\text{m}^{-1}$ , corresponding to  $qa \sim \pi$ , and a weaker peak at  $q_0 \sim 2q_0$ . The height of the strong first peak is  $S(qa \sim \pi) \sim 2.8$ , close to the value expected for a colloidal glass. Interestingly, the structure factor remains well determined even at volume fractions well above the glass transition, although the height of the first peak becomes significantly

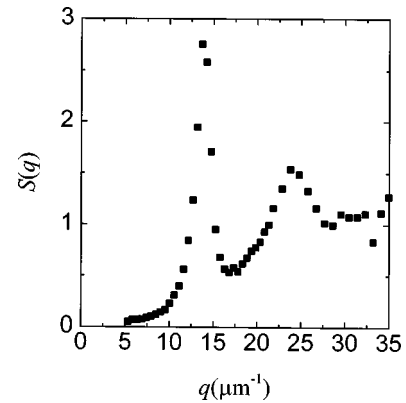


FIG. 1. (a) Static structure factor of a monodisperse emulsion with a droplet radius of  $a \approx 0.25 \mu\text{m}$  and a volume fraction of  $\phi \approx 0.54$ .

greater [13]. This reflects the fact that the disordered structure of the emulsion droplets is quenched in as the volume fraction is increased.

To probe the dynamics of the emulsion as it goes through the glass transition, we use dynamic light scattering (DLS), and collect data at values of  $qa$  below, at, and above the first peak in the structure factor, for samples whose volume fraction ranges from well below to well above the colloidal glass transition. We thereby obtain a comprehensive dynamical measure of the system as its dynamics change with increasing volume fraction  $\phi$ , and as it goes through the glass transition. We measure the intermediate scattering function (ISF)  $f(q, t) = S(q, t)/S(q)$ . Because the dynamics of the emulsion become exceedingly slow with increasing volume fractions, time averaging of the data no longer corresponds to the true ensemble average required for comparing to theoretical predictions, reflecting the nonergodicity of the system on the time scale of the measurement. Thus, during the course of a measurement, some fraction of the scattered light will fluctuate completely, while a second fraction will remain unchanged. The exact correlation function measured will depend on the relative fraction of these two contributions for the light collected by the detector. The relative contributions of the static and dynamic contributions must be properly weighted to obtain a true ensemble-averaged ISF.

Different techniques can be used to properly average the data. Perhaps the simplest is to slowly rotate the sample while the correlation function is being measured [14]. This ensures that an average over all relative contributions of static and dynamic scattering is collected. However, the motion of the sample also results in a decay of the correlation function as the speckles move across the detector, limiting the time scale over which a true decay of the sample is observed. A second method to obtain properly ensemble-averaged data entails the collection of a correlation function at a single point, and then rotating the sample more rapidly to measure the average scattered intensity; this is then used to correct the measured correlation function to obtain the ensemble-averaged ISF [15]. While this method does not directly average the data, it also does not result in any additional decay due to sample motion.

We tried both methods in these experiments; however, contrary to claims that the two techniques are equivalent [14], we found that we were able to collect considerably

better data using the latter method. The data for the samples studied here decay very slowly, requiring long collection times to observe the full extent of the decay. As a result, it was essential to measure the longest decay times possible. Using the rotation method, the limitation to measuring long decay times is set by the combination of the total duration of the experiment and by the requirement that a large number of independent speckles must be measured to obtain the average scattered intensity with sufficient accuracy to normalize the data. It is this combination of requirements that ultimately determines the slowest speed at which the sample must be rotated. Thus, for example,  $10^4$  independent speckles must be averaged to determine the average intensity to an accuracy of about 1%. Since it is quite important to accurately determine the average intensity, at least  $10^4$  speckles must be measured. For a given experiment duration, this sets the speed at which the sample must be rotated, and therefore the longest decay time that can be probed before sample motion obscures further decay. This decay time must always be significantly less than  $10^{-4}$  of the total duration of the experiment, severely limiting the decay times that can be probed in any experiment. By contrast, in the second technique, the measurement of the average intensity is separate from the measurement of the correlation function; hence the average intensity can be measured with a very high degree of accuracy by rotating the sample quite rapidly, to collect the data over a very large number of independent speckles. Then the correlation function can be measured to much longer times, without the introduction of any spurious decay due to sample motion. Although there will be increasing uncertainty in the data at these longer times, the data are nevertheless of sufficient quality to provide valuable information even at the longest delay times. Thus we found experimentally that the latter method was far better, and we used it to collect all the data presented here.

To collect our data, we typically collected static scattering for about 1 h, while the sample was slowly rotated. This provided a very accurate determination of the average static scattering. We then collected correlation functions from several different points, corrected each one individually to obtain a measure of the ensemble-averaged ISF, and finally averaged these together. We ensured that the acceptance angle of the detector was very small, so that the coherence factor, measured with the same optics as the experiments, was well above 0.9, as determined by the intercept of correlation functions from purely ergodic samples. Of course the apparent value of the intercept varied considerably for the emulsion sample, depending on the relative magnitude of the static and dynamic contributions. However, after the correction, the ISF's varied only very slightly, indicating that the averaging that we performed was sufficient.

Data collected from a series of samples, with different volume fractions ranging from  $\phi=0.54$  to 0.62 are shown in Fig. 2. For each volume fraction, we plot data obtained at three values of  $qa$ , below, at, and above the first peak of the structure factor; the  $qa$  values are indicated by arrows in Fig. 1. The  $f(q,t)$  data clearly exhibit two distinct decays on well separated time scales. Moreover, as  $\phi$  increases, the separation of these time scales also increases significantly, while the plateau in the data between the decays becomes more extended. In addition, there is a pronounced change in the

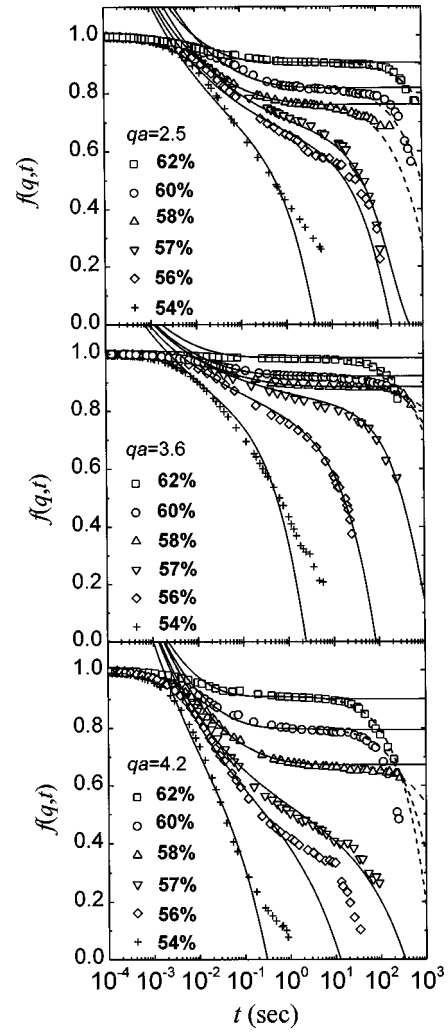


FIG. 2. Dynamic light-scattering data  $f(q,t)$  (symbols) from monodisperse emulsions collected at  $qa \approx 2.5$  (top panel), 3.6 (middle panel), and 4.2 (lower panel), for a series of volume fractions. These values of  $qa$  correspond to values of  $q \approx 10, 14.4,$  and  $16.8 \mu\text{m}^{-1}$  in the structure factor shown in Fig. 1. The lowest value of  $qa$  is below the first peak, the intermediate value is approximately at the first peak, while the highest value is above the first peak in structure factor. Fits to the data using the idealized MCT are shown by the solid lines, while the improved fits for volume fractions above the glass transition obtained with the extended MCT are shown by the dashed lines.

data between  $\phi=0.57$  and 0.58; while the volume fraction changes by only 0.01, the separation of the time scales of the two decay processes of the ISF increases by several decades, particularly at the highest  $qa$ . Nevertheless, at all values of both  $\phi$  and  $qa$ , the data always decay at the longest time scales measured. Finally, there is also a marked difference in the behavior as  $qa$  is varied; the amount of the initial decay is clearly the least for  $qa$  at the peak of the structure factor, increasing both below and above.

While the shapes of the ISF's shown in Fig. 2 are quite complex, they possess all the hallmarks expected for a system undergoing a colloidal glass transition [6–8,16]. The physical picture that accounts for the shape is that of cages formed around each particle by its neighbors. As  $\phi$  increases, any given particle becomes trapped within its cage for in-

creasing periods of time, and any relaxation mechanism for the particle to escape from its cage must become increasingly more cooperative, involving the collective motion of particles over larger distances. This cooperativity results in the pronounced slowing down of the relaxation of density fluctuations evident in the data. Qualitatively, the initial decay of the ISF corresponds to local motion of the particle within its cage, the slowly decaying plateau region corresponds to relaxation of the cage, called the  $\beta$  relaxation, while the final decay corresponds to the breakup of the cage and escape of the particle, designated as the  $\alpha$  relaxation. To quantitatively describe the data, we use mode coupling theory, which has been successfully applied to describe light-scattering data from colloidal suspensions near the glass transition [6–8,16].

Mode coupling theory describes the dynamics of a liquid approaching the liquid-glass transition through equations of motion for  $\Phi_q(t)$ , the normalized autocorrelation functions of the density fluctuations  $\rho_q(t)$ :

$$\dot{\Phi}_q(t) + \Omega_q^2 \Phi_q(t) + \int_0^t M_q(t-t') \dot{\Phi}_q(t') dt' = 0. \quad (1)$$

These equations, one for each  $q$ , are formally exact, with the important physics hidden in the memory functions  $M_q(t) = \gamma_q \delta(t) + m_q(t)$  where  $\gamma_q$  is the ‘‘regular’’ damping constant, and  $m_q(t)$  represents the slowly varying part of  $M_q(t)$ . MCT then utilizes the Mori-Zwanzig projection operator formalism and Kawasaki’s factorization approximation to express  $m_q(t)$  in terms of products of two or more other modes. In the original ‘‘idealized’’ version of MCT, only the largest such term is retained:

$$m_q(t) = \sum_{q_1, q_2} V(q, q_1, q_2) \Phi_{q_1}(t) \Phi_{q_2}(t), \quad (2)$$

where  $q_1 + q_2 = q$ , and the coupling constants  $V(q, q_1, q_2)$  are given in terms of the static structure factors  $S(q)$ ,  $S(q_1)$ ,  $S(q_2)$  which are, in turn, determined by the intermolecular potentials. For hard spheres, the coupling constants can be evaluated analytically and the coupled set of Eqs. (1) and (2) can then be solved numerically. Such solutions were obtained for both hard-sphere [17] and Lennard-Jones liquids [18]. These complete solutions to the MCT equations can, in principle, be compared directly to experimental data, providing a critical test of the theory. However, preliminary attempts to carry out such a comparison for both colloidal dispersions and emulsions have been only moderately successful; while they capture the behavior at the time scales comparable to the  $\beta$  decay, they do not properly account for the behavior at short times, and thus do not capture the full behavior of the data.

The origin of this discrepancy is that the systems modeled by these MCT expressions do not correspond exactly to the experimental colloidal or emulsion systems. Since the particles or droplets are immersed in a fluid, the diffusive motion of the particles at short time scales must be incorporated into the MCT. Recently, Mayr and co-workers have reanalyzed the hard-sphere liquid using more powerful algorithms in an attempt to do so [19]. However, in addition to the diffusive dynamics, hydrodynamic interactions between the particles also play a crucial role in determining the dynamics

at short-time scales. These interactions are not yet included in the MCT calculations, although attempts to do so are currently underway [20]. Therefore, as in all other previous comparisons of experimental dynamical data with MCT predictions, we employ the asymptotic MCT results rather than the full solutions to the MCT equations. However, in contrast to the case of hard-sphere colloids, the deformability of the emulsion droplets also affects the dynamics. To account for this, we will use the extended version of the MCT.

Near  $\phi_c$ ,  $\Phi_q(t)$ , which is assumed to be equal to  $f(q, t)$ , exhibits a two step decay, corresponding to the  $\alpha$  and  $\beta$  relaxation processes characterized by two time scales,  $\tau_\alpha$  and  $\tau_\beta$ , respectively, which are both greater than the microscopic time scale  $\tau_0$ . In the idealized version of MCT, the two decay times are well separated, and  $f(q, t)$  decays fully to zero at long times for  $\phi < \phi_c$ . In contrast, for  $\phi > \phi_c$ , the  $\alpha$  process is frozen out, leaving only the  $\beta$  process, and  $f(q, t)$  saturates to a finite value,  $f(q, \infty)$ , at long times. The transition at  $\phi_c$  signifies an ergodic to nonergodic transition that typifies a glass transition.

As  $\phi \rightarrow \phi_c$ , the divergence of  $\tau_\beta$  inherent in the MCT equations permits asymptotic expansions to be carried out that provide the MCT asymptotic results usually exploited for fitting data [7,8,16]. For  $\tau_0 \ll t \ll \tau_\alpha$ ,  $f(q, t)$  can be factorized into time- and  $q$ -dependent functions,

$$f(q, t) = f_c(q) + h(q)G(t), \quad (3)$$

where  $f_c(q)$  is the nonergodicity parameter which represents the amplitude of the arrested structure at  $\phi_c$ , and  $h(q)$  is the critical amplitude that describes the contribution of the  $\beta$  correlator,

$$G(t) = |\sigma|^{1/2} g_\pm(t/\tau_\beta), \quad (4)$$

where the master scaling function  $g_\pm(t/\tau_\beta)$  is independent of both  $q$  and concentration, and where  $\sigma = c_0(\phi - \phi_c)/\phi_c$  is the separation parameter which describes the approach to the critical volume fraction  $\phi_c$  of the glass transition. Here,  $c_0$  is a material-dependent constant. Both  $f_c(q)$  and  $h(q)$  can, in principle, be calculated from  $S(q)$  at  $\phi_c$ , and are only very weakly dependent on  $\phi$ . Volume fraction dependence enters the dynamics only through  $\sigma$ , and the two scaling times, which diverge at  $\phi_c$ ,

$$\tau_\alpha = t_0 |\sigma|^{-\gamma}, \quad \gamma = 1/2\alpha + 1/2\beta, \quad (5)$$

$$\tau_\beta = t_0 |\sigma|^{-\delta}, \quad \delta = 1/2\alpha, \quad (6)$$

where the critical exponents  $a$  ( $0 < a < 0.5$ ) and  $b$  ( $0 < b < 1$ ) are related to the exponent parameter  $\lambda$  by

$$\lambda = \frac{\Gamma^2(1-a)}{\Gamma^2(1-2a)} = \frac{\Gamma^2(1+b)}{\Gamma^2(1+2b)}, \quad (7)$$

where  $\Gamma$  is the gamma function. The final, long-time relaxation of  $f(q, t)$ , reflecting the  $\alpha$  process, is described by a second scaling law with the  $\alpha$  correlator, and can be well approximated by a stretched exponential,

$$f(q, t) = f_c(q) \exp\{-(t/\tau_\alpha)^{\beta_q}\}, \quad (8)$$

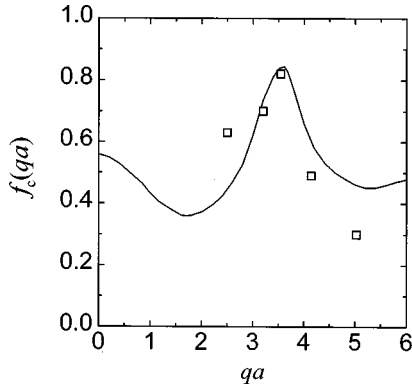


FIG. 3. Fitted values of the nonergodicity parameter  $f_c(q)$  compared with the prediction for hard spheres, shown by the solid line.

where  $\beta_q$  is the stretching exponent. Within the ideal MCT,  $\alpha$  relaxation exists only on the liquid side, where for times greater than  $\tau_\beta$ , the relaxation of the density fluctuations is shared by both the  $\beta$  and the  $\alpha$  processes, with  $\tau_\beta$  marking the crossover between the initial part of the  $\beta$  relaxation (the critical decay  $\sim t^{-a}$ ) and the von Schweidler decay ( $\sim -t^b$ ) which joins smoothly to the long-time  $\alpha$  decay [Eq. (5)]. By contrast, on the glass side, the  $\alpha$  process is arrested and the  $\beta$  process saturates at a definite value at long times.

The complete structural arrest at  $\phi_c$  predicted by the idealized MCT does not occur in simple structural glasses, where the  $\alpha$ -relaxation process moves to longer times with decreasing temperature but does not disappear. Retention of the next significant term in the memory function, beyond the leading term of Eq. (1), leads to the extended MCT [21,22]. The additional term, representing coupling to currents, is usually included through a temperature-dependent ‘‘hopping parameter’’  $\delta(T)$ . With this parameter included, much better fits to experimental data can be obtained in the transition region and in the glass phase [23,24]. For our emulsion system, the droplet deformability is physically similar to the activated hopping process underlying  $\delta(T)$ , so we will also employ the extended MCT to analyze data at concentrations above  $\phi_c$ .

### DATA ANALYSIS

To quantitatively analyze our data, we begin by calculating the  $\beta$  correlator  $G(\sigma, t)$  for hard spheres, for a trial exponent parameter  $\lambda$ , as a function of  $\phi$ . Then, for the data for each  $q$ , we approximate  $f_c(q)$  by the experimental value of the plateau of the ISF between 0.57 and 0.58, where it becomes flat. We then choose a trial value of  $h(q)$  to fit the initial decay of the data using Eq. (2). Below  $\phi=0.58$ , we combine the  $\alpha$  process using Eq. (5) with  $\tau_\alpha$  as a fitting parameter; since in the idealized MCT the  $\alpha$  process is frozen out above  $\phi_g$ , we do not include it for  $\phi>0.57$ . This fitting process is iterated for each data set to obtain the best fit to all the data. In doing this fit, we hold both  $f_c(q)$  and  $h(q)$  fixed for all  $\phi$  for each value of  $q$ , since MCT predicts that they are only very weakly dependent on  $\phi$ ; this ensures that the fit satisfies the constraints of MCT for the factorization of  $f(q, t)$ . The results of the fit are shown by the solid lines in Fig. 2. The fit to the data is very good for  $\phi<\phi_g$ ; however, at higher  $\phi$ , in the glass region, the data clearly continue to exhibit a decay

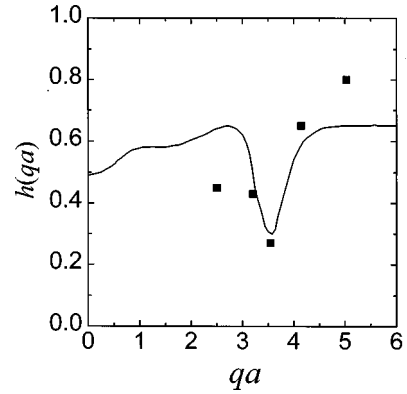


FIG. 4. Fitted values of the critical amplitude  $h(q)$  compared with the prediction for hard spheres, shown by the solid line.

at longer times, contrary to the expectations of the idealized MCT. To account for this decay, we use the extended MCT [21,22]. Within extended MCT, the final decay is also well described by a stretched exponential above  $\phi_g$  [although the simple scaling of Eq. (5) is not expected to apply], and we use this form here, choosing the value of  $\tau_\alpha$  to ensure a continuous curve through the data. With this addition, all the data are fit very well; the new fits at long times for  $\phi>\phi_g$  are shown by the dashed lines in Fig. 2. These fits are indistinguishable from the simple MCT fits at shorter times, and correctly account for the decay observed at longer-time scales.

The values obtained for  $f_c(qa)$  and  $h(qa)$  are shown in Figs. 3 and 4, respectively. The data for  $f_c(qa)$  are compared to the values predicted for hard spheres, shown by the solid line in Fig. 3. The fitted values exhibit the same trend as the prediction, with  $f_c(qa)$  exhibiting a sharp peak near the first peak in the structure factor. Similarly,  $h(qa)$  exhibits a pronounced dip near the first peak in the structure factor. In Fig. 5 we plot the  $\phi$  dependences of the fitted time scales,  $\tau_\alpha$  (circles) and  $\tau_\beta$  (squares), and compare these with the predictions of MCT for hard spheres shown by the solid and dashed lines, respectively. The agreement is again quite good. There is a pronounced divergence for  $0.57<\phi<0.58$ ,

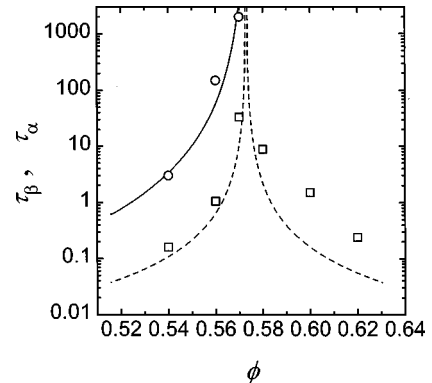


FIG. 5. The  $\phi$  dependence of the two time scales obtained from the MCT fits,  $\tau_\alpha$  (circles) and  $\tau_\beta$  (squares), compared to the predictions for hard spheres shown by the solid and dashed lines, respectively. Data for the  $\alpha$  process are shown only for  $\phi<\phi_g$ . The divergence between  $\phi=0.57$  and  $0.58$  is strong evidence of the existence of the colloidal glass transition at this volume fraction.

providing a clear measure of  $\phi_g$ . We do not show the values of  $\tau_\alpha$  obtained from the extended mode coupling fits above  $\phi_g$ . These reflect the time scales for long-time relaxation for the emulsions in the glassy state, and are in marked contrast to the behavior observed for other colloidal systems. Hard spheres exhibit no long-time decay above  $\phi_g$  [7], while soft gel spheres do exhibit a decay [9], but it cannot be described within extended MCT [10]. Thus the emulsion data are the first colloidal system that can be described by the extended MCT. This additional decay presumably arises because of the deformability of the liquid droplets [25,26]; which may enable thermal effects to cause the ultimate decay of  $f(q,t)$ , consistent with the use of a phonon-assisted hopping term. In addition, we believe that there are stresses built up within the emulsion as it is loaded into the light-scattering cell, as the observed time scale increases very slowly over the course of several weeks, indicating slow aging of the sample. Consistent with this, we observe a slow increase in the characteristic time of the final decay of the correlation function. These effects may be interesting to study as an example of the consequences of sample aging.

The asymptotic MCT equations [in contrast to the full solutions to Eq. (1)] do not account for the decay of the ISF at the shortest times where the particles are diffusing within their local cages. Furthermore, the data shown in Fig. 2 do not provide an accurate measure of this initial decay. However, some insight into this behavior can be obtained by using the same emulsion, without index matching, for diffusing wave spectroscopy which probes the very short-time motion of the particles [27]. Interestingly, for all the volume fractions shown in Fig. 2, the mean square displacement is sub-diffusive, increasing with time more slowly than linearly, even at time scales as short as 1  $\mu\text{sec}$ , and length scales of order 1  $\text{\AA}$  [25,26]. Thus the effects of the neighboring particles are felt through hydrodynamic interactions at the very shortest of time scales. This emphasizes the importance of including these interactions in any complete treatment of colloids and emulsions by the MCT.

## CONCLUSIONS

These results demonstrate the utility of these monodisperse emulsions as a new system in which to study the glass transition. Because of the flexibility of the droplets, it is a simple matter to load samples at all volume fractions, allowing the study of their properties both below and above  $\phi_g$ ; by contrast, the very long relaxation times of hard-sphere suspensions make it very difficult to work with glassy samples. Furthermore, by suitable choice of oils, emulsion droplets can be made with different indices of refraction; thus it is a simple matter to mix small concentrations of particles with the same size, but with different scattering intensities, allowing tracer measurements to be made to extend the range of these studies. Furthermore, these samples are also amenable to mechanical measurements to determine their rheological properties; these properties also exhibit all the hallmarks of a colloidal glass transition [5]. Thus this system is ideal for a detailed test of current theoretical descriptions of the glass transition. Finally, these results highlight the importance of the droplet deformability in controlling the final relaxation of the droplets. Similar long-time relaxation is expected in other systems which show glassy relaxations, such as gels or foams. These long relaxations also have a strong influence on the rheological behavior of these systems, leading to a loss modulus that is surprisingly independent of frequency [12]. Recent work has suggested that these long-time scale relaxations are directly related to the frequency independence of the loss modulus [28]. The data presented here provide a direct measure of the dynamics and the relaxations which are speculated to be essential for this unusual rheological behavior.

## ACKNOWLEDGMENTS

We thank W. Götze for helpful discussions and M. Mayr for providing numerical data from recent MCT hard-sphere computations. This work was partially supported by the NSF (Grant No. DMR96-31279) and NASA (Grant No. NAG3-2058).

- 
- [1] Dynamics of Glass Transitions and Related Topics, edited by T Odagaki, Y. Hiwatari, and J. Matsui [Prog. Theor. Phys. Suppl. **126**, R1 (1997)].
  - [2] Second International Discussion Meeting on Relaxations in Complex Systems, edited by K. Ngai [J. Non-Cryst. Solids **172-174** (1994)].
  - [3] W. Götze and L. Sjogren, Rep. Prog. Phys. **55**, 241 (1992).
  - [4] *Transport Theory and Statistical Physics: Special Issue Devoted to Relaxation Kinetics in Supercooled Liquids-Mode Coupling Theory and its Experimental Tests*, edited by S. Yip (Dekker, New York, 1995).
  - [5] T. G. Mason and D. A. Weitz, Phys. Rev. Lett. **75**, 2770 (1995).
  - [6] W. van Meegen and P. N. Pusey, Phys. Rev. A **43**, 5429 (1991).
  - [7] W. van Meegen and S. M. Underwood, Phys. Rev. Lett. **70**, 2766 (1993).
  - [8] W. van Meegen and S. M. Underwood, Phys. Rev. E **49**, 4206 (1994).
  - [9] E. Bartsch, M. Antonietti, W. Schupp, and H. Sillescu, J. Phys. Chem. **97**, 3050 (1992).
  - [10] E. Bartsch, V. Frenz, J. Baschnagel, W. Scharl, and H. Sillescu, J. Phys. Chem. **106**, 3743 (1997).
  - [11] J. Bibette, J. Colloid Interface Sci. **147**, 474 (1991).
  - [12] T. G. Mason, J. Bibette, and D. A. Weitz, Phys. Rev. Lett. **75**, 2051 (1995).
  - [13] T. G. Mason, A. H. Krall, H. Gang, J. Bibette, and D. A. Weitz, in *Encyclopedia of Emulsion Technology*, edited by P. Becher (Dekker, New York, 1996), Vol. 4, p. 299.
  - [14] J.-Z. Xue, D. J. Pine, S. T. Milner, X.-L. Wu, and P. M. Chaikin, Phys. Rev. A **46**, 6550 (1992).
  - [15] P. N. Pusey and W. van Meegen, Physica A **157**, 705 (1989).
  - [16] W. Götze and L. Sjogren, Phys. Rev. A **43**, 5442 (1991).
  - [17] U. Bengtzelius, W. Götze, and A. Sjolander, J. Phys. C **17**, 5915 (1984).
  - [18] U. Bengtzelius, Phys. Rev. A **34**, 5059 (1986).
  - [19] T. Franosch, M. Fuchs, W. Götze, M. R. Mayr, and A. P.

- Singh, Phys. Rev. E **55**, 7153 (1997).
- [20] W. Götze (private communication).
- [21] W. Götze and L. Sjogren, Z. Phys. B **65**, 415 (1987).
- [22] M. Fuchs, W. Götze, S. Hildebrand, and A. Latz, J. Phys.: Condens. Matter **4**, 7709 (1992).
- [23] H. Z. Cummins *et al.*, Phys. Rev. E **47**, 4223 (1993).
- [24] H. Z. Cummins, G. Li, W. Du, Y. H. Hwang, and G. Q. Shen, Prog. Theor. Phys. **S126**, 21 (1997).
- [25] H. Gang, A. H. Krall, and D. A. Weitz, Phys. Rev. Lett. **73**, 3435 (1994).
- [26] H. Gang, A. H. Krall, and D. A. Weitz, Phys. Rev. E **25**, 6289 (1995).
- [27] D. J. Pine, D. A. Weitz, P. M. Chaikin, and E. Herbolzheimer, Phys. Rev. Lett. **60**, 1134 (1988).
- [28] P. Sollich, F. Lecqueux, P. Hebraud, and M. E. Cates, Phys. Rev. Lett. **78**, 2020 (1997).